Kinetics of ion and prompt electron emission from laser-produced plasma

N. Farid,[1,2] S. S. Harilal,[1,a)] H. Ding,[2] and A. Hassanein[1]
[1]*Center for Materials Under Extreme Environment, School of Nuclear Engineering, Purdue University, West Lafayette, Indiana 47907, USA*
[2]*Key Laboratory of Materials Modification by Laser, Ion and Electron Beams, School of Physics and Optical Engineering, Dalian University of Technology, Dalian, China*

(Received 29 May 2013; accepted 26 June 2013; published online 29 July 2013)

We investigated ion emission dynamics of laser-produced plasma from several elements, comprised of metals and non-metals (C, Al, Si, Cu, Mo, Ta, W), under vacuum conditions using a Faraday cup. The estimated ion flux for various targets studied showed a decreasing tendency with increasing atomic mass. For metals, the ion flux is found to be a function of sublimation energy. A comparison of temporal ion profiles of various materials showed only high-Z elements exhibited multiple structures in the ion time of flight profile indicated by the observation of higher peak kinetic energies, which were absent for low-Z element targets. The slower ions were seen regardless of the atomic number of target material propagated with a kinetic energy of 1–5 keV, while the fast ions observed in high-Z materials possessed significantly higher energies. A systematic study of plasma properties employing fast photography, time, and space resolved optical emission spectroscopy, and electron analysis showed that there existed different mechanisms for generating ions in laser ablation plumes. The origin of high kinetic energy ions is related to prompt electron emission from high-Z targets. © *2013 AIP Publishing LLC*. [http://dx.doi.org/10.1063/1.4816710]

I. INTRODUCTION

Laser ablation (LA) has been an attractive field to researchers since the invention of high power lasers. With the improvement in diagnostic techniques, this field quickly drew the attention of all scientific communities including material, chemical, and biological sciences. LA and resulting plasma formation has wide spread applications such as pulsed laser deposition (PLD),[1] laser induced breakdown spectroscopy (LIBS),[2,3] laser-ablation inductively coupled-plasma mass spectrometry (LA-ICP-MS),[4] nano-particles generation,[5] laser ion source,[6,7] and table top shorter wavelength light sources for lithography[8] and microscopy.[9] However, even though LA is used for various applications, the physical parameters of laser ablation plumes vary widely with each application. The most important parameters that influence LA properties include laser wavelength, pulse width, spot size, and laser intensity.[8–11] Apart from laser properties, the target material as well as background gas nature and pressure also affect plasma plume kinetics.[12–14] Because of highly transient nature of the plume as well as wide parametric dependence, the laser ablation plume properties should be optimized properly for each application and plasma diagnostics play a key role in this regard.

The ion emission from laser produced plasma (LPP) is another emerging feature of LA which has vast applications, such as ion implantation,[15] laser driven ion accelerator,[16] and in the medical field.[17] Similar to all LA applications, laser pulse duration,[18] wavelength,[19] and power density[20] of the laser and as well as physical and chemical properties[21] of the target are the principle parameters that define the nature and type of charge particle emission from LPP. In general, ions are emitted from the solid target in the form of a cone due to their angular distribution with a preferential emission along the target normal;[22] however, laser focusing conditions also influence the flux and energy of emitted ions.[23] At the initial stage of plume expansion in vacuum, electrons overtake the ions resulting in a space charge field that accelerates ions resulting in higher velocity for more highly charged ionic states. The ions located at the front of the plasma acquire the largest energy during hydrodynamic expansion and have less interaction time for recombination processes. Faraday cup (FC)[24–26] and electrostatic energy analyzer (EEA) detectors[27,28] are routinely used for analyzing ion emission from LPP. Faraday cup ion collector provides charge integrated ion flux and temporal profiles, while EEA gives the time of flight (TOF) of various charge states. The ions angular distribution from LPP can be approximated by a single charge dependent, $\cos^n$ function, where n increases with charge state and decreases with atomic mass.[29] In general, ions with higher charge states dominate in the direction normal to the target, their concentration falls sharply away from the normal, and excited neutrals have the most angular spread.[29] This can be due to lower electron density at outer angular regions of the plume, which is effectively diminished by recombination.[10]

In this paper, we explored the kinetics of LPP ion emission generated from various targets including C, Al, Si, Cu, Mo, Ta, and W. The plasmas were created using 1064 nm, 6 ns pulses from Nd:YAG laser. A Faraday cup was used as an ion collector for determining the ion flux as well as kinetic energy distributions. The present studies revealed multiple ion structure profiles, and this is seen only for high-Z materials like Mo, Ta, and W, while single peak ion distribution was observed for low-Z materials. A detail study of ion emission from laser produced W-plasma was also carried

a)hari@purdue.edu

out using fast photography, optical emission spectroscopy, and time- and space-resolved TOF emission spectroscopy to diagnose in detail the mechanism of different types of ion emission from LPP.

II. EXPERIMENTAL DETAILS

The schematic of the experimental set-up is given in Figure 1. Briefly, an Nd:YAG laser operating at 1064 nm, which produced a maximum pulse energy of 450 mJ with a pulse of 6 ns at full width at half-maximum (FWHM) was used for generating plasma in a vacuum chamber. Seven materials consisting of metals and non-metals (C, Al, Si, Cu, Mo, Ta, W) with a purity of 99.95% were used as target materials. The target was mounted on XY translational stage, which provided fresh surface exposure for each measurement. The experiments were performed in high vacuum with base pressure of $\sim 1.0 \times 10^{-5}$ Torr. The laser beam was delivered through the window of the chamber and focused perpendicular on the sample surface using a plano-convex lens of focal length 40 cm. The estimated spot size at the target surface was 300 μm. The laser energy and hence the power density at the target surface was varied from 3.5×10^{9} to 2.4×10^{10} W cm^{-2} by using a combination of a half wave plate and cube polarizer.

Ions from LPP were monitored by a Faraday cup ion collector (IC) placed at a distance of 16 cm from the target which could be rotated from 10° to 90° with respect to target normal. A bias voltage of −30 V was applied to the ion collector, which had a 2 mm entrance aperture diameter. The IC output signal was acquired across a 50 Ω load resistor using a 5 GHz storage oscilloscope.

For fast-gated imaging, the integrated visible emission from the expanding plasma was collected through a quartz window normal to its direction of expansion using tele-photo objective lens and focused onto an intensified CCD (ICCD) camera. A gate width with 10% of sequential delay time was used. For time and space resolved measurements of plasma emission, 0.5 m triple grating (1800, 600, and 150 lines/mm) spectrograph was used. One of the exit ports of the spectrograph was coupled to an ICCD which collected the dispersed spectral features of the plasma. The other exit port was coupled to a photomultiplier tube (PMT) with 2 ns rise time. A diverter mirror was used to switching detectors. A programmable timing generator was used to control the delay time between the laser pulse and the detector system. All the spectrally resolved and TOF optical emission spectroscopy studies were performed perpendicular to the direction of plasma expansion. The optical system which consisted of two lenses with a one-to-one correspondence was used to image the plasma plume onto the entrance slit (30 μm) of spectrograph.

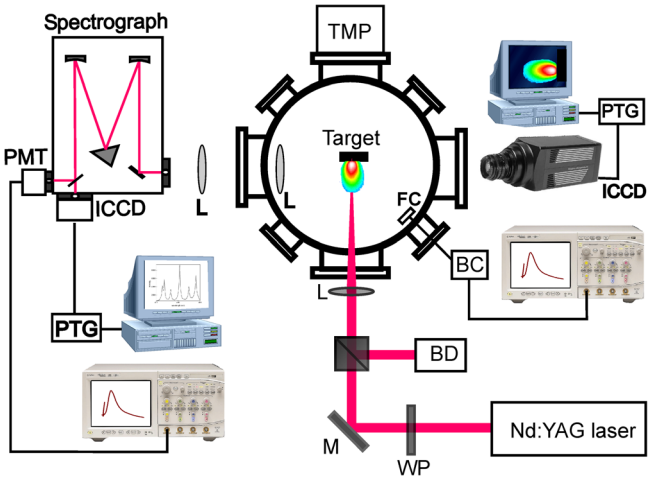

FIG. 1. The schematic of the experimental setup. TMP, turbomolecular pump; PTG, programmable timing generator; PMT, photomultiplier tube; ICCD, intensified charged coupled device; WP, half waveplate; M, laser mirror; FC, Faraday cup; BC, biasing circuit; BD, beam dump; L, lens.

III. RESULTS AND DISCUSSION

A. Ion analysis

The study of ion emission from LPP especially in vacuum is essential to understand the hydrodynamic expansion of the plume. The ion kinetic energy features and angular distribution along with the flux are important parameters that define the plume expansion dynamics. The ion emission features from seven targets (C, Al, Si, Cu, Mo, Ta, W) comprised of metals and non-metals were investigated. The ion collector was placed at an angle of 20° and at a distance of 16 cm from the target. A bias voltage of −30 V was applied to collect the ions and was also sufficient to repel electrons.

TOF ion profiles obtained from the FC for various elements are shown in Figure 2. A laser power density of 2.4×10^{10} W cm^{-2} was used to record the ion profiles. It can be seen that the ion profile is strongly dependent on atomic mass of elements. The peak of each profile corresponds to the maximum probable arrival time of ion flux into the collector. The ion emission from all elements studied showed a broad peak whose arrival time is found to be dependent on atomic mass; the peaks are shifted to longer delay times with increasing the atomic mass. These broad peaks can be approximated by a shifted Maxwell-Boltzmann (SMB) distribution indicating these ions may be thermalized. Comparing the various elements studied, only high-Z metals (Mo, Ta, and W) exhibit multiple ion TOF profiles. The observations of low intensity peaks at short time delays before occurrence of the broad main peak are probably due to fast ions component. Therefore, emitted ions from the high-Z material may be divided into two groups: (i) fast ions and (ii) slow ions. The origin of these fast ions will be discussed later. In general, the lighter elements have sharp and narrower profiles while the heavier elements have less intense and wider ion distribution. It is observed that ion flux strongly depends on the atomic mass as well as on sublimation energy as shown in the Figure 3.

For lighter elements, the ion flux decreases abruptly with increasing target-Z; however, the ion flux reduction is not as steep for mid- and high-Z elements. The log–log dependence of the ion flux from metals as well as for semiconductor (Si) with respect to sublimation energy is shown Figure 3(b). The results showed the ion flux decreases with increasing sublimation energy which is consistent with the work of Baraldi *et al.*,[21] where they used 193 nm laser

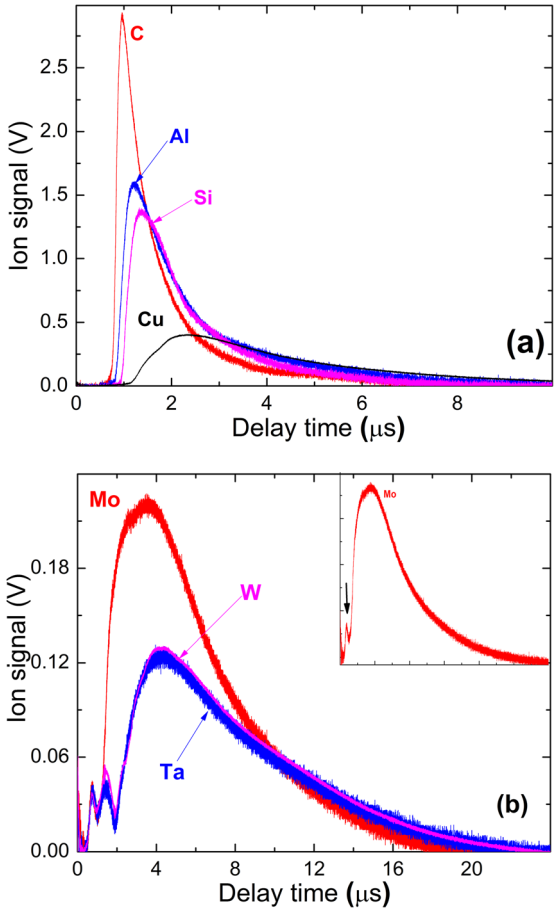

FIG. 2. Typical ion TOF signal obtained from IC is given for various target materials (a) C, Al, Si, and Cu and (b) Mo, Ta, and W. For obtaining this data, the FC was positioned at 16 cm from the target surface and at an angle of 20° to the target normal. The laser power density used was 2.4×10^{10} W cm^{-2}. The inset in (b) shows Mo ion profile which has only one peak for fast ions (indicated by arrow mark).

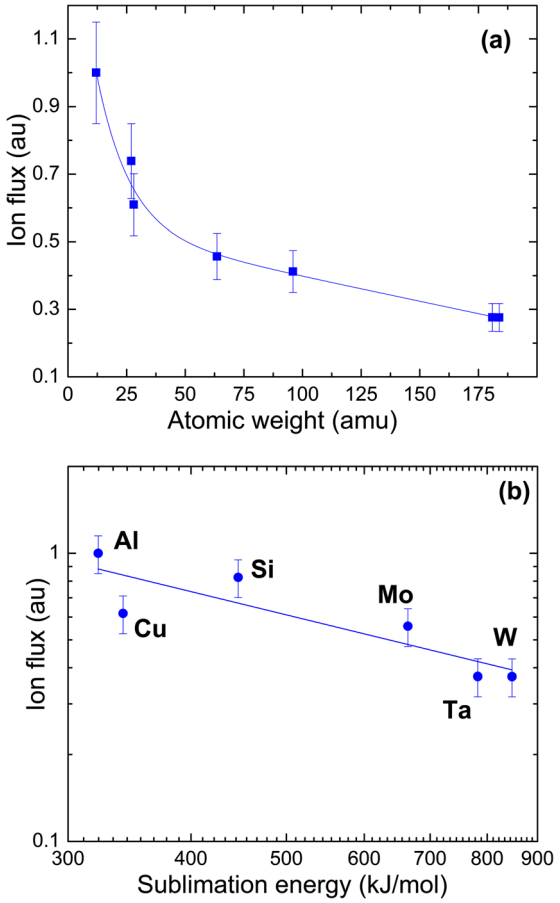

FIG. 3. Ion flux of C, Al, Si, Cu, Mo, Ta, and W from laser-produced plasma in vacuum with a power density of 2.4×10^{10} W cm^{-2} as a function of atomic mass is given in (a). The log-log plot of ion flux and metal sublimation energy is given in (b).

ablation of various metal targets and observed a linear log-log dependence between ion flux and melting temperature.

The velocity of the ion profiles obtained from TOF data as a function of atomic mass is shown in the Figure 4. Similar to the ion flux data, the ion velocity is also found to decrease with atomic mass (M) for all elements studied. The maximum probable velocity of ions emanating from plasmas follows the $M^{-0.5}$ dependence as shown in the inset of Figure 4(a). In Figure 4(b), kinetic energy profiles are given for comparison between lighter and heavier elements in the energy range up to 8 keV. The energy distribution becomes broader with the increasing atomic mass and the maximum probable KE shifts to the lower end. In the case of W, one group of fast ions have a KE of 10 keV and second group has KE of 40 keV which is about 10 and 40 times higher than the slow ions as shown in the inset of Figure 4(b).

We have seen multiple peak TOF ion profiles for high-Z elements like W. These profiles have been reported recently especially for the W ions and explained by the cause of impurities like H^+, C^+, O^+, and hydrocarbon ions.[30,31] However, our studies showed that the origin of fast ions is not simply caused by impurities on the surface based on following reasons. Figure 5 presents TOF ion signals correspond to different number of shots from laser produced W-plasma at the same target location. The given intensity of first shot signal was reduced by a factor of 20 for comparison. The ion signal obtained from C plasma is also given for comparison. All signals were obtained by placing the IC at an angle of 20° with respect to the target normal and at a distance of 16 cm from the target. The laser power density was kept constant at 2.4×10^{10} W cm^{-2}. We observed a fast single peak profile from the fresh W target (similar to low-Z ions) as shown in Figure 5(a) after the first laser shot.

Low-Z material contamination on target surface is unavoidable and a low-power laser pulse can be used to clean the surface. However, after the first laser shot, the ion profile generated from contamination is no longer present and consistent TOF profiles were recorded for multiple shots (2–50) at the same target location. Moreover, it is also clear from Figure 5 that multiple profile structures were not observed in the ion signal from first laser shot. From the second laser shot onwards, consistent multiple ion profiles are observed. This suggests that the signal from first shot was from surface impurities and after this cleaning shot, the ion profiles were entirely emanating from W plasma. The mismatch in the delay time and in the number of shots (Figure 5(b)) rules out the contamination reason for the generation of multiple profiles. To understand the origin of the multiple

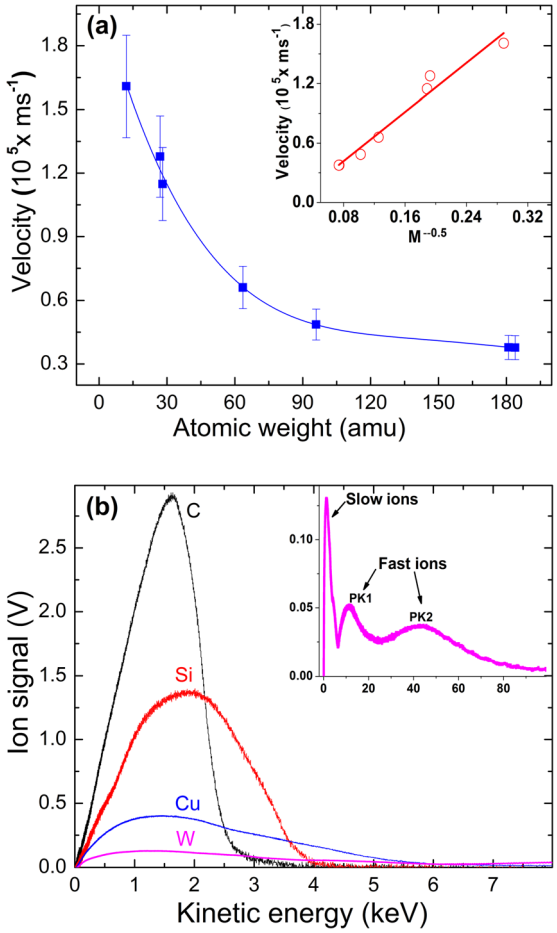

FIG. 4. (a) Ion velocity for different elements as a function of atomic weight. The inset shows the ion velocity dependence on $M^{-0.5}$. (b) KE profiles for C, Si, Cu, and W are given in the energy range up to 8 keV. The inset in (b) gives the high KE peaks of fast ions (labeled 1 and 2) from W plasma.

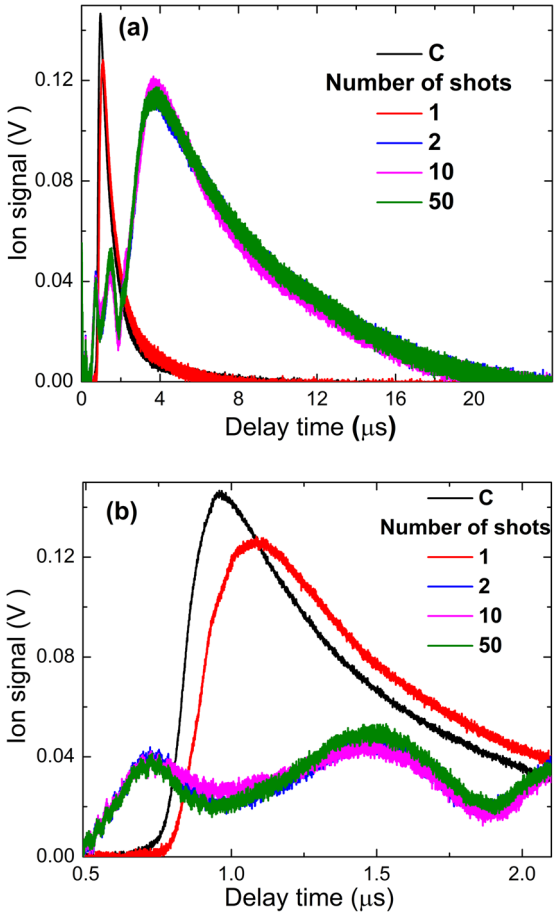

FIG. 5. (a) TOF ion signal from W-plasma with different number of pulses along with TOF signal of C ions and (b) magnification of fast ions peaks. An Nd:YAG laser operating at 1064 nm with a power density of 2.4×10^{10} W cm^{-2} was used to produce the plasma, and ion collector was placed at an angle of 20° and 16 cm from the target normal. The ion signal obtained from W during first shot and C ion signals were scaled down for better view.

ion profile structure a more detailed study is required. Hence, we evaluated the role of laser power density as well as angular features of the W ions profile.

The W ion TOF profiles recoded at different laser power density levels in the range of 3.5×10^9 to 2.4×10^{10} W cm^{-2} are shown in Figure 6(a). As expected, the ion flux increases with increasing laser power density. The positions of the peaks were also shifted to shorter delays with increasing laser power density indicating enhancement of the average energy of the ions. In nano-second LPP, the leading part of the laser pulse interacts with the target surface, which leads to the formation of energetic plume, and the remaining part of the beam is utilized to heat up the plume. In other words, after the generation of the plasma, the target is shielded from the remaining part of the direct laser beam because of laser absorption in plasma due to inverse bremsstrahlung. This laser plasma interaction eventually heats up the plasma, and more highly charged ions are produced.

The coupling between the incoming laser and evolving plasma becomes more effective with higher power densities and the ions located in the front of the plume gain more energy and accelerate. The increment in the fast ions signal with the laser energy indicates that these fast ions are not solely due to impurities on the surface. Ion flux for slow as well as the fast ion group also increases linearly with the increase in power density as shown in Figs. 6(b) and 6(c). It was observed that the KE increased from 0.6 to 1.6 keV for slow, from 18.8 to 42.0 keV for fast ions correspond to Pk1 and from 5.4 to 11.0 keV for fast ions correspond to Pk2 as the laser intensity was varied from 0.3 to 2.4×10^{10} W cm^{-2}. Across the investigated power density range, a sevenfold increase in power density resulted in an enhancement of the KE of approximately 2.6 for slow ions and 2.2 for fast ions (Fig. 7).

In order to explore the angular distribution of the ion flux, the IC was placed at various angles with respect to the target surface normal, and TOF ion signals were recorded. Figure 8 shows the angular distribution of flux for slow and fast ions. The solid lines given in Figure 8 correspond to Gaussian fit. The angle resolved integrated flux distribution showed a different trend for slow and fast ions. The flux of slow ions is peaked about the target normal. However, two different and independent angular distributions for fast ions are identified. First, a fast ion (Pk2) emission with a similar distribution to slow ions with a maximum flux around target normal, second, fast ions (Pk1) with a smaller cone with a peak flux around 30°. This fast ion group appeared after the

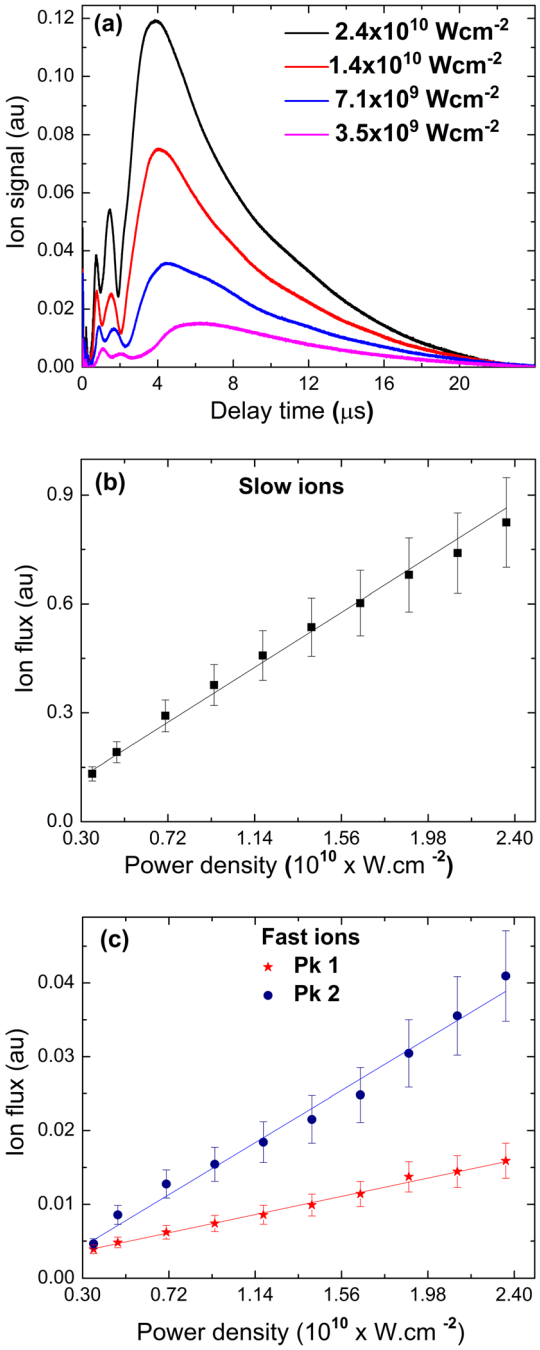

FIG. 6. The dependence of ion signal on laser power density is given in (a) for W plasma. The changes in W slow ion flux with respect to laser power density are given in (b) and the respective changes for fast ion peaks are given in (c).

first shot and remain, independently on the number of laser shot and angle of collection.

FC ion signal provided interesting results with multiple peak ion distributions for high-Z materials. Ion emission study from LPP under different power densities also showed the enhancement in flux, velocity, and hence KE for both fast ions and slow ions, but it is difficult to explain with great certainty the reasons for the occurrence of multiple peak structures using FC analysis alone. In order to further investigate the plasma propagation and ion dynamics, we carried out fast photography and optical emission spectroscopy

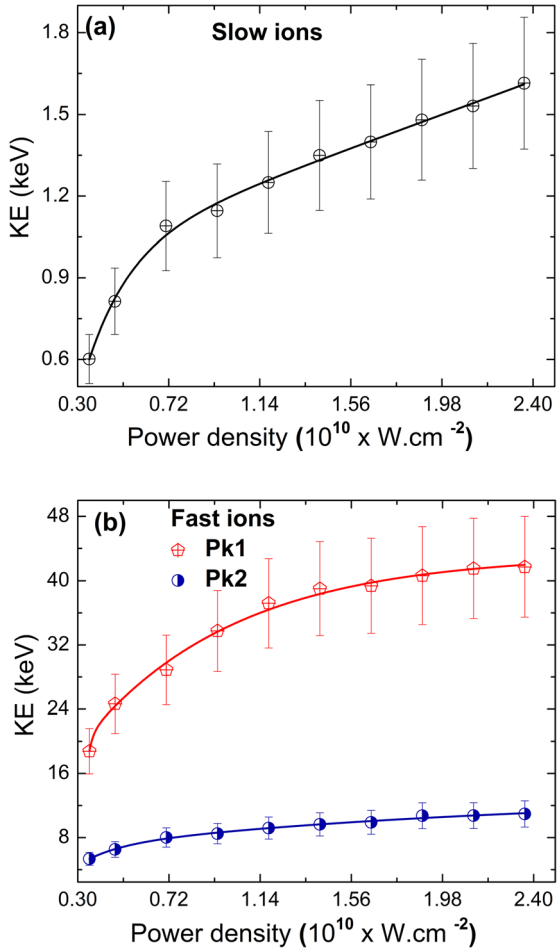

FIG. 7. (a) KE corresponds to maximum IC signal for slow and (b) fast ions with laser power density.

studies of W plasma. Most of the lower-charged ions emit in the visible region; therefore, a fast photography and time-of flight optical emission spectroscopy of W ions will be useful tools in this regard.

B. Fast photography

The laser power density used in the present studies is 3.5×10^9 to 2.4×10^{10} W cm^{-2} and under these irradiance conditions prominent ion emission from LPP are expected to be from lower-charged ions. These lower-charged ions emit strongly in the visible region, and fast gated imaging employing ICCD is a versatile plasma diagnostic tool for mapping 2D expansion of transient plumes. We captured and evaluated visible emission features of W plasma for verifying the existence of multiple components in the plume. Plume splitting is typically observed when the LPP is expanding into an ambient where gas phase collisions transforms the initial distribution.[32] However, it should be noted that the multiple peak distribution for W ion profiles are observed in vacuum.

Figure 9 presents the evolution of laser produced plasma recorded by an ICCD camera at different delays with respect to the peak of the laser pulse with a gate width of 10% of the delay time. The laser power density used for this measurement was 2.4×10^{10} W cm^{-2}. The images clearly indicate

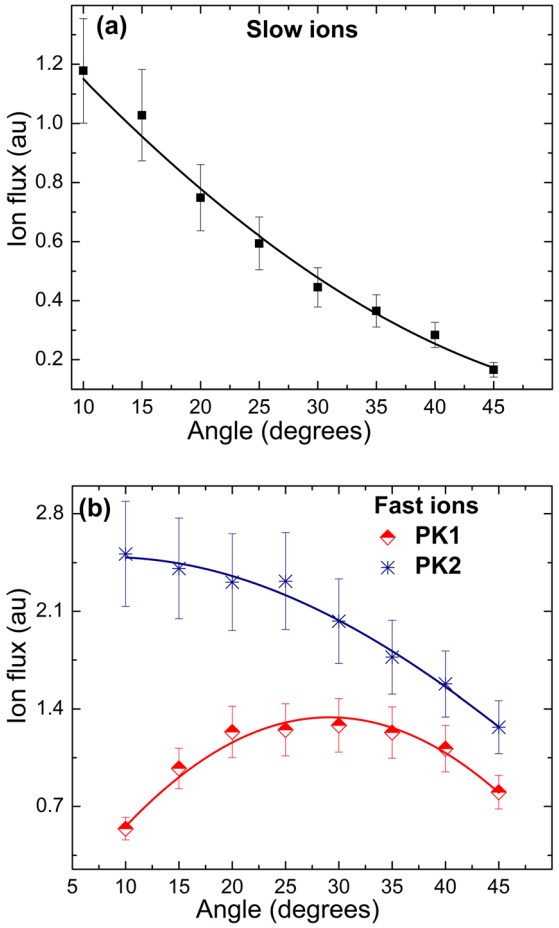

FIG. 8. Angle resolved flux of slow (a) and fast ions (b) from laser-produced W-plasma with a 2.4×10^{10} W cm^{-2} power density. Ions were collected at an angle of 20° from the target normal.

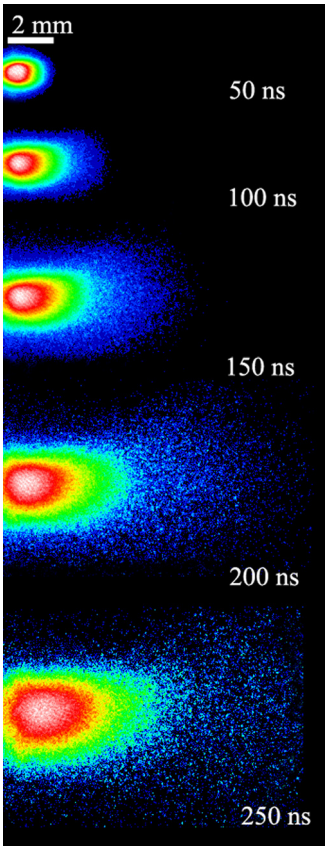

FIG. 9. Temporal evolution of the W-plasma produced by Nd:YAG laser (1064 nm) with a power density of 2.4×10^{10} W cm^{-2} at a pressure of 1.0×10^{-5} Torr. The plume emission was recorded by the ICCD camera with a gate width of 10% of the delay time.

the plume expand freely in vacuum with no evidence of plume oscillations at early times. Spectrally integrated ICCD self-emission images can give insights about the dynamics of the plasma expansion. In order to study the expansion velocity of emitting species in the plasma plume, we have plotted the plume front position (R) versus time delay (t) and results are given in the Figure 10. The R-t plot showed the plume was expanding freely in vacuum indicated by linear line fit (solid line in Figure 10). A mean velocity of 2.3 $(\pm 0.34) \times 10^4$ ms^{-1} was derived from this plot, which is comparable with the velocity of slow ions determined from the IC signal. However, ICCD images did not show the presence of fast ions, which were traveling with kinetic energies of 40–100 keV based on IC analysis. This is not surprising considering the ions contributed by fast ions are <3% of total ion population.

C. Optical emission spectroscopy studies

To further elucidate the behavior of W plume evolution, optical time-of-flight (OTOF) studies have been carried out. The OTOF provides very useful information about the history of certain species at a specific location in the plume with high temporal precision.[33] Typical temporal evolution of W^+ line at 357.24 nm recorded at various distances is given in Figure 11. The time evolution of the spectral emission profiles obtained in vacuum clearly reveals that the W^+ species ejected by the tungsten plasma exhibits a twin-peak TOF distribution. These peaks are not resolved near the target but well separated beyond certain distance from the target due to plasma propagation. The kinetic distributions of OTOF peaks resemble the TOF profiles obtained from IC. The first peak corresponds to the emission of fast ions and second to the slow ions from plasma core. The R-t plots obtained from the OTOF are given in Figure 11(b) for both

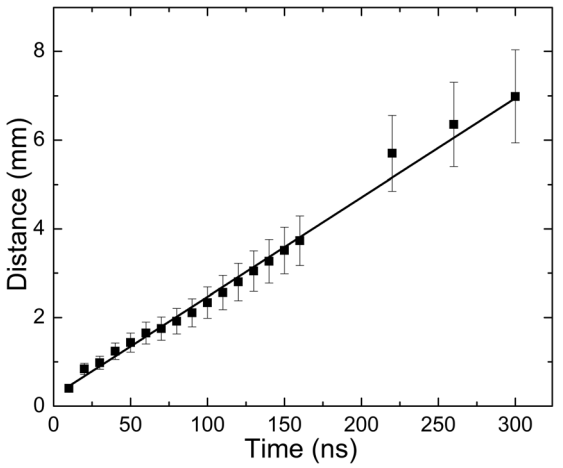

FIG. 10. R-t plot obtained from time resolved ICCD self-emission images. The solid line in the figures corresponds to the linear fit.

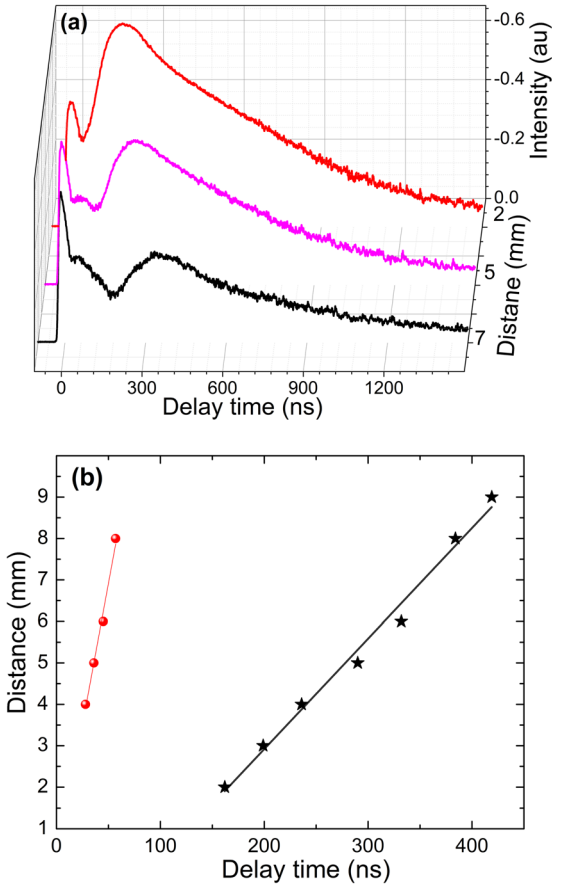

FIG. 11. (a) Optical emission time-of-flight profiles of W^+ (357.24 nm) at different distances from target; (b) R-T plot of peak intensity times versus distance for fast and slow ions for velocity measurement.

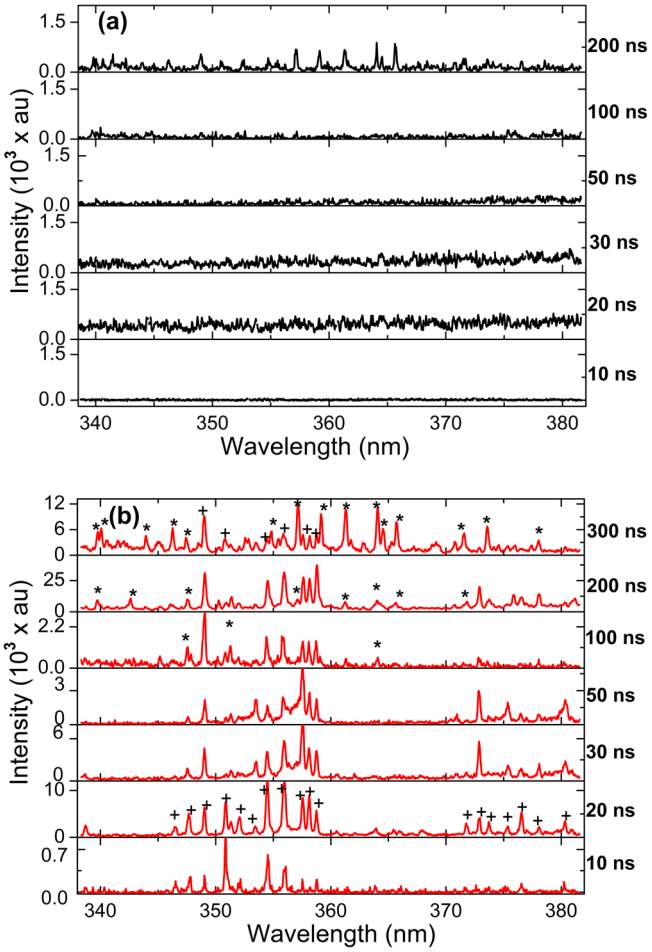

FIG. 12. Time resolved spectra of W-plasma produced in (a) vacuum and in (b) ambient atmosphere of Ar at a pressure of 100 mTorr. All the spectra were recorded with a gate width of 5 ns and at distance of 6 mm from the target. Ar^+ and W lines are represented by * and + symbols.

faster and slower ion components and followed a linear dependence. The measured values of velocities of fast ions ($1.4 \pm 0.21 \times 10^5\,ms^{-1}$) as well as the slow ions ($2.7 \pm 0.40 \times 10^4\,ms^{-1}$) from the OTOF are in consistent with values measured from TOF IC signal.

The results of OTOF and TOF IC studies are in good agreement with the emission of fast and slow ions. However, the exact mechanisms leading to the formation of fast ions are still unclear. The interaction of these fast moving ions with a background gas may be useful to understand their origin if the observed fast ions are capable of exciting or ionizing ambient gas species in the vacuum chamber. Therefore, we inserted Ar background gas in the vacuum chamber with pressures ~100 mTorr and recorded emission spectra at various times after the onset of plasma generation.

Figure 12 represents the time resolved emission spectra of W-plasma recorded at a distance 6 mm from the target surface in vacuum and in the presence of 100 mTorr Ar gas. The spectra were obtained with a gate width of 5 ns. In vacuum, no emission from the W-plasma was detected at early times even though weak continuum emission was evident. The W lines started to appear after 200 ns time delay at a distance of 6 mm. Before the appearance of W lines, a weak continuum was observed at 20 ns, which disappeared at later times. The spectral features observed in the presence of 100 mTorr Ar ambient is given in Figure 12(b), and it showed strong presence of Ar^+ lines even at the earliest times. Ar^+ emission lines identified are marked in Figure 12 with *, while the W lines are with +. Interestingly, at early times, the spectral features are entirely dominated by Ar^+ ions, and at later times, emission from W lines also appeared. This is not surprising considering the velocity of W ions obtained from ion analysis or OTOF. Based on the velocity estimate from OTOF analysis, the W ion peak will appear ~200 ns after the onset of plasma at 6 mm, and this is consistent with spectral data. It indicates that the laser plasma from W is preceded by partially ionized ambient gas plasma. We also evaluated the existence of ambient plasma for low-Z target materials such as C and Al and no evidence for a stationary background plasma before the arrival of target plasma.

Excitation and ionization of ambient gas at early time before the arrival of plasma has been reported previously and explained by the prompt electrons.[34] We recorded the electron profiles from the plasma using the Faraday cup. Figure 13 shows the electron profile from the W-plasma recorded using the positive biasing of FC. To record the electron signal, +20 V applied to FC and was placed at an angle of 20° at a distance of 16 cm from the target. The electron signal showed a sharp peak at the earliest time indices followed by a broad distribution. The first sharp peak observed

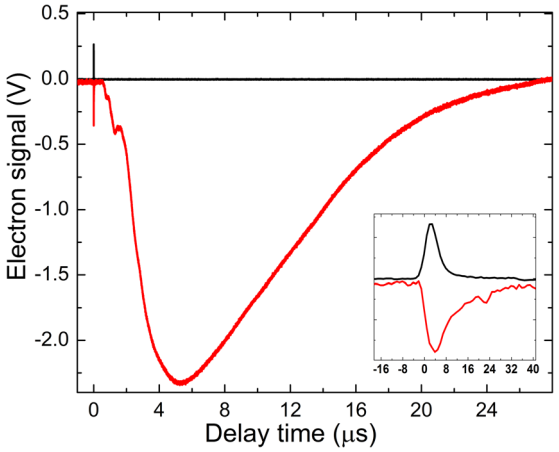

FIG. 13. Time of flight profile of the electron signal from laser produced W-plasma. The first sharp peak is due to prompt electrons and second broader peak corresponds to electrons emission from core plasma. The inset shows that prompt electron emit during the laser pulse duration and its width exactly matches with the laser pulse.

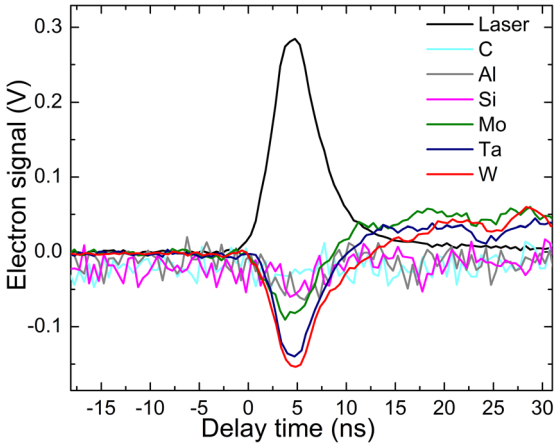

FIG. 14. Faraday cup electron signals along with the ion signal for high-Z elements. This timescale highlights the short duration of the "prompt electron" signal.

at the earliest time could be due to prompt electrons and the second broader peak corresponds to electrons emission from core plasma. The inset shows that prompt electron emit during the laser pulse duration and its width almost matches the laser pulse. According to Figure 13, the prompt electrons are travelling with high velocities and these electrons could be responsible for ambient gas excitation and ionization.

There exists, however, some controversy on the origin of these prompt electrons during a nanosecond laser-matter interaction.[35] For example, Amoruso *et al.*[36] observed highly energetic prompt electrons using EEA during 248 nm laser ablation of Al target and explained as these prompt electrons are generated due to two photon photoelectric effects during the laser pulse. Similar kinetic distribution of fast electrons was observed by Issac *et al.*[34] during Nd:YAG laser ablation of Ag and attributed to laser heated electrons escaping from the interaction volume before the lattice absorbed the energy. Cronberg *et al.*[37] suggested that the origin of the high kinetic energies was due to collisional inverse bremsstrahlung absorption experienced by photo emitted electrons.

The existence of prompt electrons for W plasma could also be responsible for generating fast ions in the earliest times. The temporal profiles of these electrons follow approximately the time duration of the laser pulse. However, we noticed the presence of fast ions only for high-Z materials like Mo, Ta, and W. In case of high-Z elements, a large number of electrons are available in the conduction band, which results in a higher flux of prompt electrons at the initial times of laser pulse interaction with the target surface. Then, these electrons absorb the laser photons energy through the inverse bremsstrahlung process reaching energies suitable to induce ionization processes.[38] Hence, electrons emanating from the high-Z material at early times will have high flux which may lead to generation of fast electrons because of the Coulomb effect as well as deriving excitation and ionization of the ambient molecules and atoms.

Surprisingly, we observed fast ions only for high-Z materials and not for low-Z material like C, Al, etc. In order to investigate the effect of target-Z on prompt electron generation, we analyzed the electron signal of different materials used in the present studies and results are shown in Figure 14. Results show that the measured prompt electron signals are greatly depended on atomic mass of the element, stronger signal are observed for high-Z materials, and the electron signals are found to be weaker for low-Z materials like C, Al, etc. This can be correlated with observation of faster ions in the IC signal as well as existence of ambient plasma before the arrival of target plasma. Hence for high-Z metal targets, prompt electrons possess significantly higher flux compared to low-Z targets, which may lead to higher electric fields and resulting space charge separation between prompt electrons and initially emitted ions. This can accelerate a fraction of ions with higher kinetic energies. The existence of multiple faster ion peaks for W and Ta in comparison with single faster peak for Mo could be due to the availability of a large number of electrons in the conduction band for high-Z metals like W and Ta. Hence, the prompt electron flux will be higher during the initial times of interaction between the laser and the target. Some of these prompt electrons may get further acceleration through the inverse bremsstrahlung process causing electrons with slightly different kinetic energies which may lead to generation of fast ions with differing kinetic energies. However, more detailed studies are needed to explain the observed two-fast ion peaks of the high-Z targets under the given conditions.

IV. CONCLUSIONS

We investigated ion emission features of LPP from various targets comprised of metals and nonmetals (C, Al, Si, Cu, Mo, Ta, and W). The plasmas were produced by focusing fundamental radiation from a Nd:YAG laser beam. An ion collector was employed to obtaining TOF signal that was used to determine the flux, velocity, KE, and angular distribution of emitted ions. Ion flux was found to strongly depend on the atomic mass as well as on the sublimation energy. The reduction in ion flux is steeper with increasing mass for lighter elements; however, the ion flux reduction is not as steep for mid- and high-Z elements. For metals, the ion flux is found to be function of sublimation energy. The ion

velocity was also found to decrease with atomic mass M and showed $M^{-0.5}$ dependence. A comparison of temporal ion profiles of various materials, under the conditions studied in this work, showed only high-Z elements exhibited multiple structures in the ion TOF profiles indicated by the observation of faster kinetic energy peaks which were absent for low-Z element targets. The slow ions seen regardless of the target material atomic number propagated with kinetic energy of 1–5 keV, while the fast ions observed in high-Z materials possessed significantly higher energies (20–40 keV).

TOF ion emission studies of W-plasma showed the existence of two groups of ions: fast group of ions with lesser flux and a slow ion group with higher flux but less energy. Significant enhancements were observed in ion flux as well as the KE with increasing laser power density. This could be caused by increased laser-plasma interaction and hence plume heating at higher power densities. An enhancement in KE of about 2.6 times for slow ions and 2.2 times for fast ions was noted with about 7 times enhancement in laser power density. The angle resolved emission study pointed out that the slow ions have a peak flux around the target normal.

The plume hydrodynamics expansion features investigated using ICCD imaging clearly pointed out the free expansion of the plume in the vacuum. The optical emission TOF spectroscopy of W^+ revealed the existence of a twin-peak TOF distribution. The measured velocities from OTOF profile indicated that these profiles are similar to the multiple peak structure observed with ion TOF studies employing the Faraday cup. We also evaluated the W plasma properties in vacuum as well as in the presence of 100 mTorr Ar gas. Excitation and ionization of ambient Ar gas at early time before the arrival of plasma was observed. The spectral features recorded at a distance of 6 mm from the target showed strong presence of Ar^+ emission lines. The analysis of electrons showed significant presence of prompt electrons especially for high-Z target materials like W, and the presence of ambient plasma before the arrival of target plasma is explained due to the excitation and ionization of ambient gas by prompt electrons. The presence of prompt electrons as well as the higher flux of fast electrons for high-Z targets indicates that these electrons could be responsible for the generation of fast ions from the high-Z materials.

ACKNOWLEDGMENTS

This work was partially supported by the U.S. National Science Foundation PIRE program.

[1]D. B. Chrisey and G. K. Hubler, *Pulsed Laser Deposition of Thin Films* (John Wiley & Sons Australia, Limited, 1994).
[2]D. A. Cremers and L. J. Radziemski, *Handbook of Laser-Induced Breakdown Spectroscopy* (Wiley, 2006).
[3]S. S. Harilal, G. V. Miloshevsky, P. K. Diwakar, N. L. LaHaye, and A. Hassanein, Phys. Plasmas **19**, 083504 (2012).
[4]J. J. Gonzalez, A. Fernandez, D. Oropeza, X. Mao, and R. E. Russo, Spectrochim. Acta, Part B **63**, 277 (2008).
[5]S. Amoruso, R. Bruzzese, N. Spinelli, R. Velotta, M. Vitiello, X. Wang, G. Ausanio, V. Iannotti, and L. Lanotte, Appl. Phys. Lett. **84**, 4502 (2004).
[6]E. Woryna, P. Parys, J. Wołowski, and W. Mróz, Laser Part. Beams **14**, 293 (1996).
[7]P. Yeates, J. T. Costello, and E. T. Kennedy, Rev. Sci. Instrum. **81**, 043305 (2010).
[8]S. S. Harilal, T. Sizyuk, A. Hassanein, D. Campos, P. Hough, and V. Sizyuk, J. Appl. Phys. **109**, 063306 (2011).
[9]S. S. Harilal, G. V. Miloshevsky, T. Sizyuk, and A. Hassanein, Phys. Plasmas **20**, 013105 (2013).
[10]A. E. Hussein, P. K. Diwakar, S. S. Harilal, and A. Hassanein, J. Appl. Phys. **113**, 143305 (2013).
[11]S. Mahmood, R. S. Rawat, Y. Wang, S. Lee, M. Zakaullah, T. L. Tan, S. V. Springham, and P. Lee, Phys. Plasmas **19**, 103504 (2012).
[12]F. Rezaei and S. H. Tavassoli, Phys. Plasmas **20**, 013301 (2013).
[13]N. Farid, H. Wang, C. Li, X. Wu, H. Y. Oderji, H. Ding, and G.-N. Luo, J. Nucl. Mater. **438**, 183 (2013).
[14]S. Mehrabian, M. Aghaei, and S. H. Tavassoli, Phys. Plasmas **17**, 043301 (2010).
[15]E. Woryna, J. Wolowski, B. Kralikova, J. Krasa, L. Laska, M. Pfeifer, K. Rohlena, J. Skala, V. Perina, F. P. Boody, R. Hopfl, and H. Hora, Rev. Sci. Instrum. **71**, 949 (2000).
[16]M. Borghesi, J. Fuchs, S. V. Bulanov, A. J. Mackinnon, P. K. Patel, and M. Roth, Fusion Sci. Technol. **49**, 412 (2006).
[17]A. Yogo, K. Sato, M. Nishikino, M. Mori, T. Teshima, H. Numasaki, M. Murakami, Y. Demizu, S. Akagi, S. Nagayama, K. Ogura, A. Sagisaka, S. Orimo, M. Nishiuchi, A. S. Pirozhkov, M. Ikegami, M. Tampo, H. Sakaki, M. Suzuki, I. Daito, Y. Oishi, H. Sugiyama, H. Kiriyama, H. Okada, S. Kanazawa, S. Kondo, T. Shimomura, Y. Nakai, M. Tanoue, H. Sasao, D. Wakai, P. R. Bolton, and H. Daido, Appl. Phys. Lett. **94**, 181502 (2009).
[18]T. Cummins, T. Otsuka, N. Yugami, W. Jiang, A. Endo, B. Li, C. O'Gorman, P. Dunne, E. Sokell, G. O'Sullivan, and T. Higashiguchi, Appl. Phys. Lett. **100**, 061118 (2012).
[19]J. R. Freeman, S. S. Harilal, B. Verhoff, A. Hassanein, and B. Rice, Plasma Sources Sci. Technol. **21**, 055003 (2012).
[20]D. Campos, S. S. Harilal, and A. Hassanein, Appl. Phys. Lett. **96**, 151501 (2010).
[21]G. Baraldi, A. Perea, and C. N. Afonso, J. Appl. Phys. **109**, 043302 (2011).
[22]B. Verhoff, S. S. Harilal, and A. Hassanein, J. Appl. Phys. **111**, 123304 (2012).
[23]E. Woryna, P. Parys, J. Wolowski, J. Krasa, L. Laska, B. Kralikova, M. Pfeifer, K. Rohlena, and J. Skala, Laser Part. Beams **17**, 307 (1999).
[24]R. Janmohamed, G. Redman, and Y. Y. Tsui, IEEE Trans. Plasma Sci. **34**, 455 (2006).
[25]D. Doria, A. Lorusso, F. Belloni, and V. Nassisi, Rev. Sci. Instrum **75**, 387 (2004).
[26]P. Hough, P. Hayden, C. Fallon, T. J. Kelly, C. McLoughin, P. Yeates, J. P. Mosnier, E. T. Kennedy, S. S. Harilal, and J. T. Costello, J. Phys. D: Appl. Phys. **44**, 355203 (2011).
[27]D. Margarone, L. Torrisi, A. Borrielli, and F. Caridi, Plasma Sources Sci. Technol. **17**, 035019 (2008).
[28]P. Yeates, C. Fallon, E. T. Kennedy, and J. T. Costello, Phys. Plasmas **18**, 103104 (2011).
[29]T.-J. Andrea and R. Klaus, J. Phys. D: Appl. Phys. **32**, 2827 (1999).
[30]B. Ilyas, A. H. Dogar, S. Ullah, N. Mahmood, and A. Qayyum, Laser Part. Beams **30**, 651 (2012).
[31]J. Wolowski, L. Celona, G. Ciavola, S. Gammino, J. Krasa, L. Laska, P. Parys, K. Rohlena, L. Torrisi, and E. Woryna, Lasers Part. Beams **20**, 113 (2002).
[32]S. S. Harilal, C. V. Bindhu, M. S. Tillack, F. Najmabadi, and A. C. Gaeris, J. Appl. Phys. **93**, 2380 (2003).
[33]K. F. Al-Shboul, S. S. Harilal, and A. Hassanein, Appl. Phys. Lett. **100**, 221106 (2012).
[34]R. C. Issac, P. Gopinath, G. K. Varier, V. P. N. Nampoori, and C. P. G. Vallabhan, Appl. Phys. Lett. **73**, 163 (1998).
[35]S. S. Harilal, B. O'Shay, Y. Tao, and M. S. Tillack, J. Appl. Phys. **99**, 083303 (2006).
[36]S. Amoruso, M. Armenante, R. Bruzzese, N. Spinelli, R. Velotta, and X. Wang, Appl. Phys. Lett. **75**, 7 (1999).
[37]H. Cronberg, M. Reichling, E. Broberg, H. B. Nielsen, E. Matthias, and N. Tolk, Appl. Phys. B **52**, 155 (1991).
[38]F. Caridi, L. Torrisi, D. Margarone, and A. Borrielli, Laser Part. Beams **26**, 265 (2008).